Effect of Deformation on Hydrogen Trapping and Effusion in TRIP–Assisted Steel

Joo Hyun Ryu[a], Young Soo Chun[c], Chong Soo Lee[c], H. K. D. H. Bhadeshia[a,b], Dong Woo Suh[a]

[a]*Graduate Institute of Ferrous Technology, POSTECH, Republic of Korea*

[b]*Materials Science and Metallurgy, University of Cambridge, U.K.*

[c]*Materials Science and Engineering, POSTECH, Republic of Korea*

Abstract

The trapping of hydrogen at a variety of sites in multiphase transformation–induced plasticity (TRIP) steels has been characterised using thermal desorption spectroscopy and the results have been modelled using diffusion theory. It is discovered that austenite serves as a reversible trapping site which is more potent than grain boundaries or dislocations in ferrite. Plastic deformation which leads to the partial martensitic transformation of the austenite results in an alteration in the trapping condition of the inherited hydrogen. It is demonstrated that these phenomena can be incorporated into a mathematical model which permits the desorption of hydrogen to be predicted quantitatively as a function of, for example, the heating rate, phase fractions, and phase transformation. An interesting outcome is that the mechanical degradation of the steel by hydrogen is more pronounced in TRIP steel containing austenite which is relatively less stable to martensitic transformation during deformation. This is because the phase transformation causes a reduction in the trap binding energy, thus enhancing the apparent mobility of the hydrogen.

Keywords: hydrogen, TRIP steels, retained austenite, trapping energy

1. Introduction

Hydrogen is legendary in its ability to harm the toughness of steels [1, 2] and its role in static failure, i.e., unexpected failure after a component has been in service for a period well below its design life [3]. Resistance to hydrogen–induced static fracture now is a basic acceptance criterion in the exploitation of TWIP steels [4], strong automotive–steels [5, 6], and is a suspect in the occurrence of early failures in large bearings for wind turbines [7].

TRIP–assisted steels consist predominantly of allotriomorphic ferrite with 15–30% of carbon–

---

enriched retained austenite; the latter can undergo martensitic transformation during the course of plastic deformation. Of all the steels susceptible to embrittlement, the role of hydrogen in the TRIP steels is particularly unclear [5] because the deformation mechanism involves displacive transformation which not only leads to changes in the fractions of microstructural constituents, but also generates defects which are potential hydrogen trapping sites. Any hydrogen inherited by the martensite will have quite different solubility and diffusivity when compared with the parent austenite.

Thermal desorption spectroscopy (TDS) is commonly used to follow the evolution of hydrogen from a variety of sources within the steel as the sample is heated at a constant rate. Hydrogen atoms which are more strongly bound to traps evolve at higher temperatures so that the resulting spectrum can be interpreted to reveal information about the sources. Previous work on hydrogen–charged TRIP–assisted steels has largely involved qualitative interpretations of TDS spectra [8–10]. The present work is an investigation of the release of hydrogen from TRIP–assisted steels, both experimentally using TDS and with a theoretical interpretation which permits the desorption spectrum to be predicted as a function of deformation, phase transformation and heating rate.

2. Experimental Details

Alloys

Table 1 lists the chemical compositions of two alloys, L–Al and H–Al, which are TRIP–assisted steels when appropriately heat treated. Vacuum induction–melted ingots of dimensions $300 \times 150 \times 50$ mm were reheated at $1200\,^{\circ}$C for 2 h and hot–rolled to 4.5 mm in thickness with finishing temperature above $800\,^{\circ}$C followed by air cooling to room temperature. The alloys were cold–rolled to 1 mm in thickness after pickling in a 10 % HCl solution and then intercritically annealed using an infrared furnace at 720 (L–Al) and $780\,^{\circ}$C (H–Al) respectively for 2 min. The heating and cooling rates were $10\,^{\circ}$C s^{-1}. This gives both alloys a comparable retained austenite content, albeit of different mechanical stabilities [11]. A third treatment, H–Al 900, involved annealing to $900\,^{\circ}$C in order to produce a structure without retained austenite; the detailed microstructures and mechanical properties have been presented elsewhere [11].

Microstructural characterisation

The microstructure was observed using a field emission gun scanning electron microscope (FE–SEM) equipped with an electron back–scattered diffraction (EBSD) facility. In the latter case the specimens were finally mechanically polished with a colloidal silica suspension and the step size was $0.07\,\mu$m. The retained austenite was determined using X–ray diffraction with $Cu\,K_{\alpha}$ radiation; the samples in that case were finally chemically polished in a 5% HF + H$_2$O$_2$ solution. Integrated intensities of 110_{α}, 200_{α}, 211_{α}, 220_{α}, and 111_{γ}, 200_{γ}, 220_{γ}, 311_{γ} reflections were used for the quantitative phase fraction measurements [12].

Hydrogen charging and thermal desorption

Tensile test coupons with a 32 mm parallel length, 6 mm width and 1 mm thickness were prepared according to the ASTM [13], polished with the 800 SiC grit papers and charged electrochemically with the hydrogen for periods between 1–72 h in an aqueous mixture of 3% NaCl+0.3% NH$_4$SCN at 0.5 A m^{-2}. Charging for 72 h was found sufficient to saturate the samples. Thermal desorption spectroscopy with gas chromatography was conducted at constant heating rates of 100–300 °C h^{-1} to a maximum temperature of 500 °C. The parallel length part of each charged–tensile sample was cut immediately after charging and placed in the TDS furnace. The sample gas was analysed at 5 min intervals using helium as a carrier gas and the desorption rate was defined as the amount of hydrogen evolved in 1 min per gram of the specimen. A standard mixture He + 10.2 volume ppm of H$_2$ was used for the calibration. It is noteworthy that hydrogen–induced surface damage or cracking was not observed even after charging at the highest current density of 30 A m^{-2}. The hydrogen contents of the tensile specimens were evaluated with a duplicated sample prepared under the same condition.

Mechanical tests

Slow strain rate tensile tests were conducted on the specimens charged with hydrogen at a constant crosshead speed of 0.015 mm min^{-1}, corresponding to a nominal strain rate of 10^{-5} s^{-1}. A faster strain rate of 10^{-2} s^{-1} was used to examine the dynamic transition of trapping sites during deformation.

3. Results and Discussion

Microstructure

Fig. 1 illustrates representative microstructures; the austenite fractions in L–Al and H–Al are 0.26 and 0.30 respectively. L–Al alloys contains recovered ferrite with low–misorientation boundaries, H–Al has a fully recrystallised structure. The coarse ferrite grains in H–Al originate from its large Al content, which results in an expanded two-phase region of ferrite and austenite at the hot–rolling temperature. Fig. 1c confirms that the H–Al 900 specimen has a negligible retained austenite content because of the higher annealing temperature of 900°C.

As will be discussed later, the mechanical stability of retained austenite is related to the degradation of mechanical properties by hydrogen in these multiphase steels. The mechanical stability in terms of the decrease in austenite content as a function of plastic strain, is illustrated by the solid symbols in Fig. 2. The austenite in H–Al is significantly more stable than that in L–Al; the reasons for this are described elsewhere [14] but the apparent stability depends on the austenite composition, grain size and the partitioning of strain between the phases during the course of deformation.

Hydrogen effusion

Fig. 3 shows the TDS spectra for samples hydrogen–charged using a current density of $0.5\,\mathrm{A\,m^{-2}}$; the desorption rate increases with the charging time, but hardly changes beyond a charging time of 60 h for L–Al and H–Al and 12 h for H–Al 900. The temperature of maximum desorption rate (T_P) is mostly less than 100°C, suggesting the release of hydrogen from reversible trap sites [15]. Since the desorption profiles and T_P do not change after prolonged charging, it is assumed for those cases that a steady state distribution of hydrogen is established within the specimens.

Fig. 3b,d indicate another desorption peak above 400°C for all the specimen, irrespective of the charging condition or the amount of retained austenite. The trapping there is regarded to be irreversible and not considered in the present study because such hydrogen does not lead to a deterioration of mechanical properties [16]. Fig. 4a confirms that the diffusible hydrogen content is almost constant after 60 h of hydrogen charging for L–Al and H–Al alloys and 12 h for H–Al 900. The faster saturation of H–Al 900 specimen than L–Al or H–Al alloys is attributed to the absence of retained austenite, for two reasons, that the diffusivity of hydrogen at $323\,\mathrm{K}$ in ferrite is 3–4 orders of magnitude greater than in austenite [17] and the secondly hydrogen is 10 times more soluble in austenite than in ferrite [18]. This is consistent also with the greater saturation hydrogen contents (4 and 5.4 ppmw in L–Al and H–Al respectively) of the samples containing retained austenite. One discrepancy is that the austenite fraction in H–Al alloy is greater by 15% but the saturation hydrogen is higher by 35%; it is suggested that this is because the fine recrystallised grains in H–Al with their large misorientation boundaries provide additional trapping sites [19].

The interpretation of the data described above is difficult, given the multiphase character of the samples. To separate the desorption from austenite, samples of L–Al and H–Al were charged to saturation at $1\,\mathrm{A\,m^{-2}}$ for 72 h, then aged at ambient temperature for 168 h in order to allow any diffusible hydrogen with the non–austenitic regions to escape; calculations based on $\sqrt{6Dt}$ using a published diffusion coefficient (D) for hydrogen in ferrite [18] over $t = 168\,\mathrm{h}$ indicate a diffusion distance in excess of 360 mm, far greater than the 0.5 mm half–thickness of the sheet samples studied. This assessment was confirmed by the fact the mobile hydrogen in H–Al 900 completely diffused out within 24 h of ageing at ambient temperature, Fig. 4b.

Fig. 5 shows the results from the charged and aged samples. It is normal to analyse TDS spectra for activation energies by studying the change in T_P as a function of heating rate using the Kissinger equation [20] with the additional assumption of a first–order reaction. We also attempted to do this but the activation energies thus derived did not adequately represent the shapes of the desorption curves. This is because the Kissinger equation does not represent the physical events appropriate for such experiments, where we have hydrogen diffusing out of the free surfaces of the 1 mm steel sample used. First–order kinetics of the type described by the Kissinger analysis are more appropriate for cases where the reaction occurs homogeneously throughout the assembly so that specimen dimensions are not relevant. Another analytical model [21] reasonably represents the effusion of hydrogen from a sheet sample assuming that the steel is single phase, but as admitted by the authors, its application

to actual TDA spectra has not yielded promising fits, presumably because of assumptions regarding trap densities and characteristics in samples which are single–phase. To deal with this, Fick's first law of diffusion was applied in a stepwise manner to calculate the flux J emerging from each broad surface of the steel sheet, with the implicit assumption that the sample has a sufficiently small half–thickness for this simple equation to apply:

$$J = -D_0 \exp(-Q/RT) \times \frac{c - c_e}{x} \qquad (1)$$

where c is the concentration within the steel, c_e is that outside the steel, taken to be zero, and x is a distance which determines the gradient of concentration. D_0 and Q are the pre–exponential term and activation energy respectively, of an effective diffusion coefficient. Two factors need to be taken into account in applying this equation, the first that TDS analysis involves continuous heating, and the second that the composition within the steel changes as the hydrogen effuses out. The calculation was therefore done in 1°C steps, with a modification of T and c at each step, in the latter case correcting the concentration within the steel to account for the hydrogen that had escaped. It should be noted that the analyses presented below begin with samples which are saturated with hydrogen, so that there should not be gradients of concentration within the steel, other than those associated with the distribution of hydrogen between phases.

When considering the escape of hydrogen from austenite into the environment of the TDS equipment, it is necessary to account for the fact that the austenite is not continuous through the steel but is present as clusters of grains. It can, however, be assumed that the controlling feature is the concentration gradient within the austenite since any hydrogen that leaves the austenite can diffuse much more rapidly through the ferrite. It is reasonable then to set x as a measure of the size of the austenite regions. To analyse the data, the diffusion coefficient used was that measured for austenite, i.e., $D_0 = 7 \times 10^{-7} \, \mathrm{m^2 \, s^{-1}}$ and $Q = 48 \, \mathrm{kJ \, mol^{-1}}$, [22]; it is important to note that this coefficient is determined using independent permeability experiments rather than an analysis of activation energy using the Kissinger equation on TDS data.

The analysis using the stepwise application of equation 1 was then applied to the charged and aged data for $100 \, \mathrm{°C \, h^{-1}}$, allowing x to be a fitting parameter. The distance x was in this way determined to be $12 \, \mathrm{\mu m}$, which is not an unreasonable value considering the size of the clusters of austenite grains in Fig. 1. Using this value of x, and without changing any other parameter, predictions were made for the heating rates 200 and $300 \, \mathrm{°C \, h^{-1}}$. The results are illustrated in Fig. 6a,b and the predictions of the unfitted higher heating rate data are gratifying, although with some discrepancies at the highest of temperatures.

To test the basis of this analysis further, a saturation–charged and unaged sample of L–Al, which has less mechanically stable austenite, was deformed to a 10% plastic strain after which the fraction of austenite that survived was only 0.013. In such a case the diffusion distance must be set to the half–thickness of the steel sheet. Using this value of x but allowing D to be fitted for the $100 \, \mathrm{°C \, h^{-1}}$ heating rate, gave the fit illustrated in Fig. 6c, with $D_0 = 2.3 \times 10^{-4} \, \mathrm{m^2 \, s^{-1}}$ and $Q = 39 \, \mathrm{kJ \, mol^{-1}}$. Not surprisingly, this represents a much faster diffusion rate than in austenite but is nevertheless dramatically less than expected

for ferrite where the activation energy should be about $7\,\text{kJ}\,\text{mol}^{-1}$ [18]. This is because the hydrogen is trapped at defects, and the observed activation energy of $Q = 39\,\text{kJ}\,\text{mol}^{-1}$ is well within the range of reported values for the binding energy of hydrogen at defects such as dislocations, i.e., 27–$58\,\text{kJ}\,\text{mol}^{-1}$ [2, 23]. Once again, good agreement was obtained when the fitted values of D_0 and Q were used to predict the desorption curves for the two greater heating rates, giving confidence in the analysis.

Simultaneous effusion from traps and austenite

The data used in the preceding analysis are summarised in Table 2; they define the separated data for the trapping of hydrogen in austenite (derived from charged and aged samples) and at defects within the ferrite (derived from deformed material). It now becomes possible to use these to interpret multiphase effects where the TDS spectra of saturation charged samples containing both retained austenite and traps within the ferrite, but it is necessary to partition the total hydrogen into these two sites. Fig. 7 shows the deconvolution of the $100\,^{\circ}\text{C}\,\text{h}^{-1}$ data into hydrogen evolving from traps in the ferrite and that from austenite. This was achieved by best fitting the experimental data to assumed values of the concentrations of hydrogen at traps (c_α) and in austenite (c_γ), with $c = c_\alpha + c_\gamma$, but taking all other values as listed in Table 2. The values of these concentrations are

Sample	c_α / ppmw	c_γ / ppmw
L–Al	2.5	3
H–Al	4	5

With these values fixed, it is possible to predict reasonably well the corresponding TDS curves for the other two higher heating rates as illustrated in Fig. 7.

Some of the austenite will undergo martensitic transformation when the steel is plastically deformed, but if it is assumed that the amount of hydrogen trapped in austenite is proportional to its fraction, then it should be possible now to predict the TDS curves for samples which are deformed, charged and subjected to desorption analysis. However, there have been suggestions that hydrogen influences the stability of retained austenite in severely charged samples [24–26]. It was therefore felt necessary to first investigate whether the decomposition of austenite depends on the hydrogen concentration, but it is in fact found that there is no significant dependence in the alloys studied, as illustrated in Fig. 2.

The analysis presented in Fig. 8 shows that without any fitting parameters beyond those already described, and the retained austenite data from Fig. 2, it becomes possible to predict the TDS spectra of samples which have been deformed, saturation charged and then heated at $100^{\circ}\text{C}\,\text{h}^{-1}$.

Tensile properties and trap transfer

Fig. 9 shows the slow strain–rate tensile test results for L-Al and H-Al samples as a function of the amount of pre–charged hydrogen. There is the expected decrease in ductility with

increasing hydrogen content but interestingly, no significant change in the work hardening behaviour. This is expected, since as shown above (Fig. 2), the hydrogen does not influence the stability of the austenite. Furthermore, the effect of hydrogen on solid solution strengthening at ambient temperature is rather small ($< 35\,\text{MPa}$) [27], which probably is within the scatter expected in the strong steels studied here.

Austenite transforms into martensite during deformation, thereby transferring hydrogen into less potent trapping sites, thus leading to easier diffusion of hydrogen. This should lead to an enhanced deterioration in ductility specifically in TRIP–assisted steels as compared with those that do not transform as a function of plastic strain. The transfer of hydrogen was proven by conducting tensile tests using a higher strain rate of $10^{-2}\,\text{s}^{-1}$, to minimise the loss of hydrogen during testing. The ductility increases because of a competition between hydrogen mobility and plastic deformation [28]. This was confirmed in the tensile tests (Fig. 10a,b); the austenite fractions for the high strain rate samples at a strain corresponding to fracture, decreased to 0.05 and 0.20 in L–Al and H–Al respectively . The accompanying TDS results in Fig. 10c,d are quite revealing, where samples which were charged before straining, charged after straining, and those without straining, were subjected to TDS analysis. They prove conclusively that the deformation–induced decomposition of the austenite places the hydrogen into regions where it has a greater diffusivity.

4. Conclusions

The desorption of hydrogen from multiphase TRIP–assisted steels with different austenite mechanical stabilities has been studied using thermal desorption analysis. The work shows that the hydrogen dissolved in austenite can be regarded as trapped given the large activation energy of diffusion, which is greater than that of generic traps found within the ferrite and martensite. As a consequence, the deformation–induced martensitic decomposition of the austenite leaves the inherited hydrogen in a more mobile state. This is likely to have a greater detrimental effect on mechanical properties than in a comparable steel without transforming austenite, although this particular statement has not been experimentally verified in the present work.

A simple analysis has been presented of thermal desorption spectra which accounts for specimen size and can be utilised to predict quantitatively the behaviour of hydrogen in steels containing austenite and ferrite, as a function of changes in phase fractions.

The algorithm for the calculation of thermal desorption spectra according to the simple theory described here is available for download at www.msm.cam.ac.uk/map/steel/tar/hydrogen_effusion.zip

7

Table 1: Chemical compositions (wt%) of alloys

	C	Mn	Si	Al
L–Al	0.12	4.6	0.55	1.1
H–Al	0.12	5.8	0.47	3.1

Table 2: Parameter values derived from present work. α and γ represent ferrite and austenite respectively. The values of x are specific to the present work, with x_γ being the size of austenite clusters in the mixed structure, and x_α the steel sheet half–thickness in a fully ferritic sample.

Comment	D_0 / $\mathrm{m^2\,s^{-1}}$	Q / $\mathrm{kJ\,mol^{-1}}$	x / mm
Reported values for H dissolved in γ	7×10^{-7}	48	0.012
Fitted values for H at defects in α	2.3×10^{-4}	39	0.5
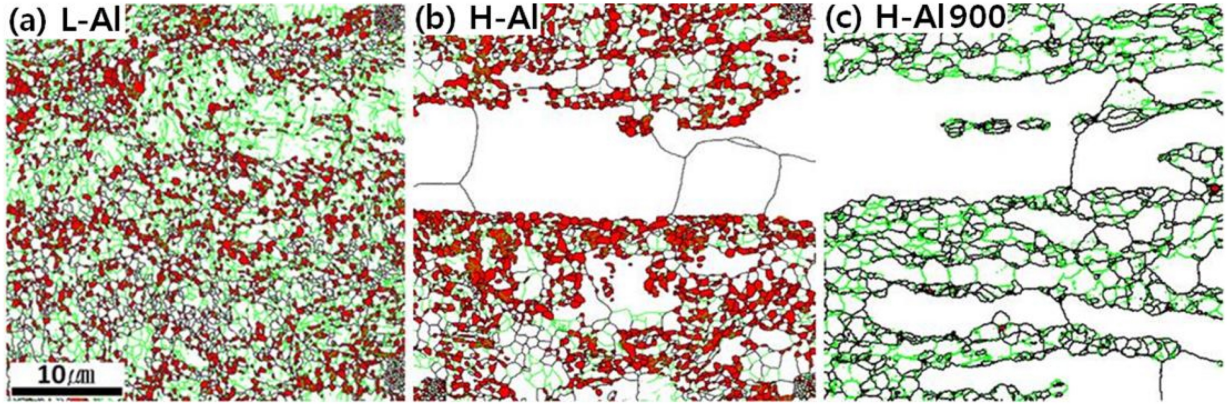
Figure 1: EBSD phase mappings of (a) L–Al , (b) H–Al and (c) H–Al 900 in which ferrite and austenite is represented by white and red, respectively. Green lines indicate low–misorientation (2–15°) boundaries whereas black lines represent high–misorientation boundaries.
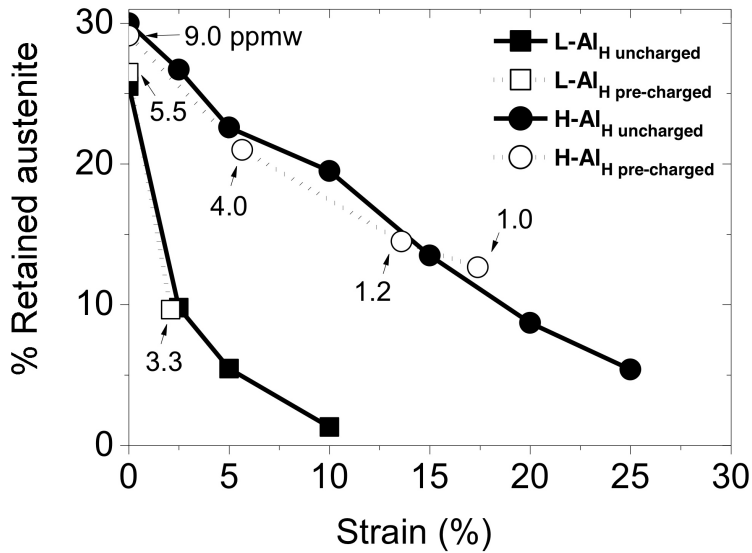
Figure 2: Solid symbols show the mechanical stability of austenite in samples H–Al and L–Al. The open symbols are discussed later in the paper, to illustrate that the mechanical stability of the retained austenite in the alloys studied does not depend on the hydrogen concentration.
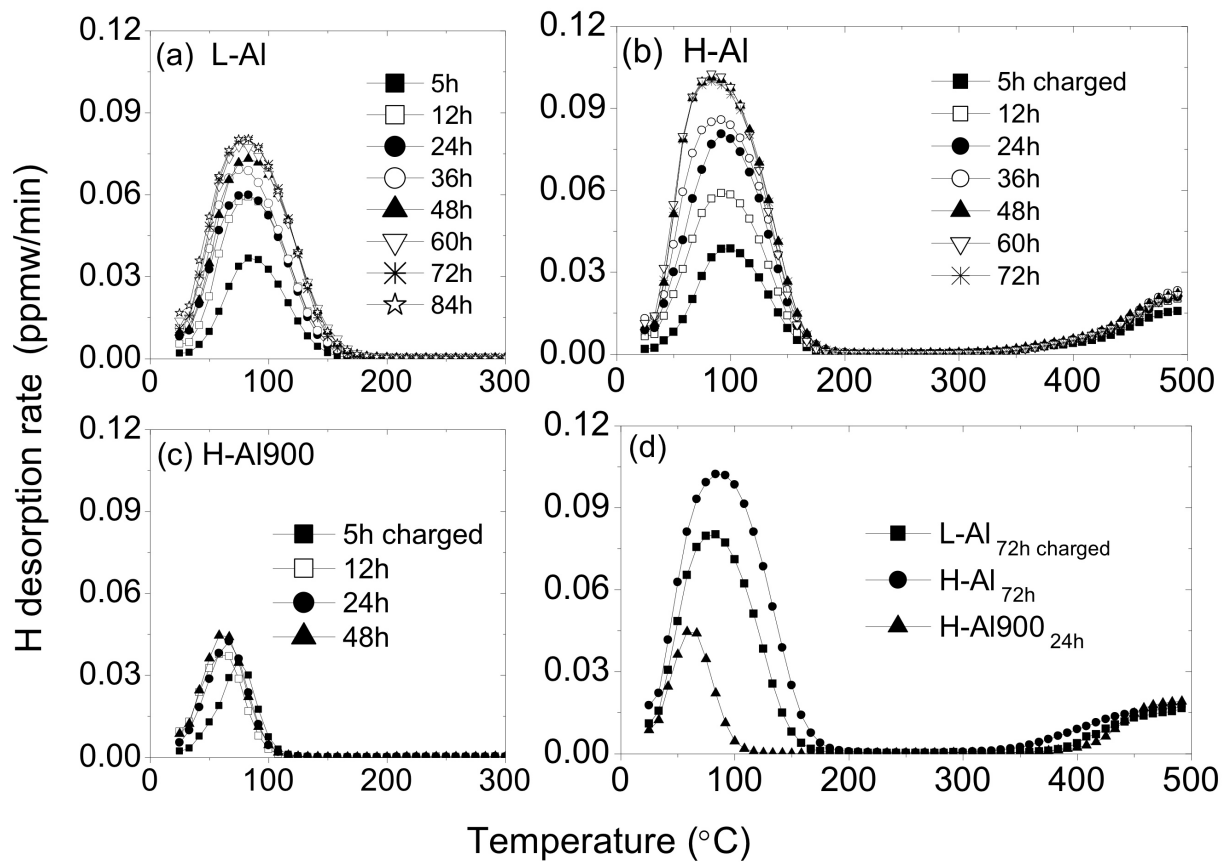
Figure 3: Thermal desorption profiles of (a) L–Al , (b) H–Al and (c) H-Al 900 as a function of hydrogen charging time. (d) Comparison of desorption profiles for samples charged to saturation.
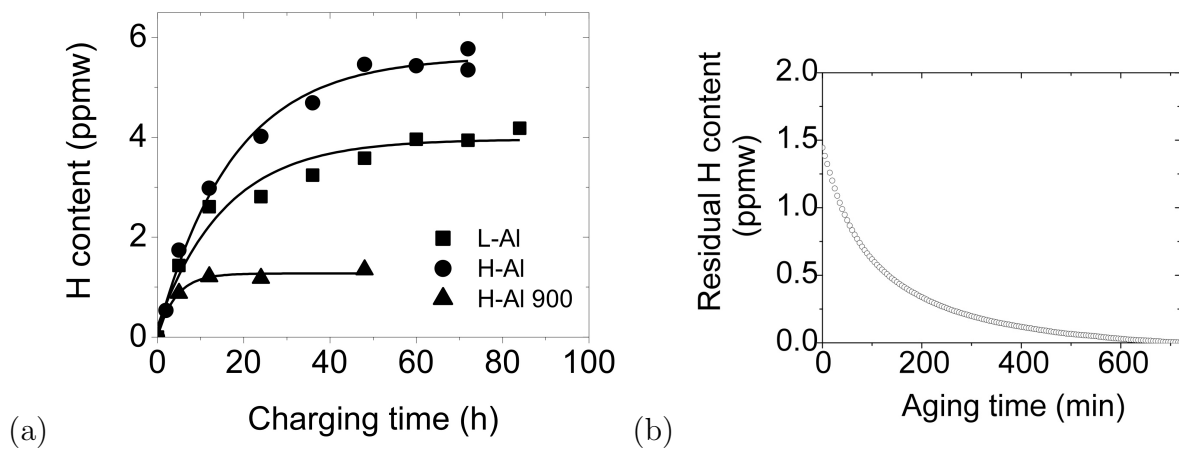
Figure 4: (a) Total diffusible hydrogen content as a function of charging time. (b) Mobile hydrogen in H–Al 900 is completely removed in less than 24 h of ageing at ambient temperature.
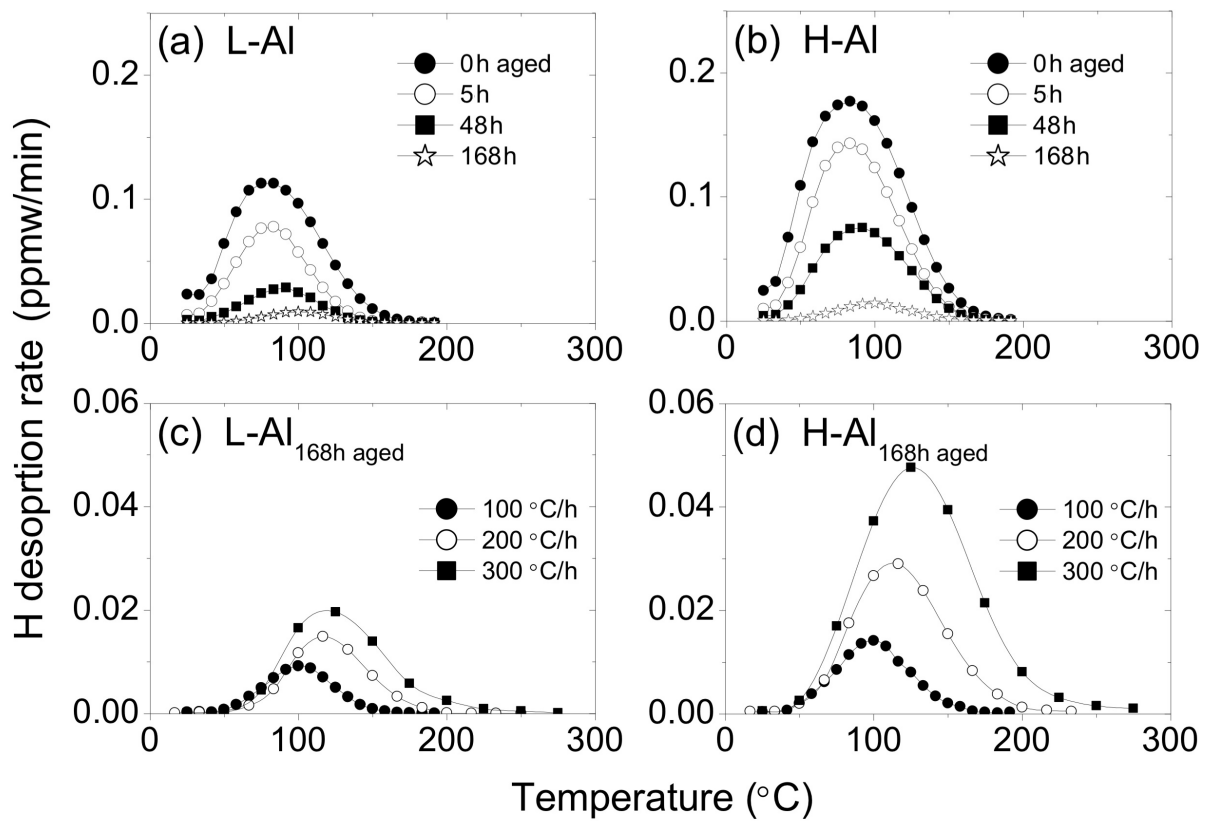
Figure 5: A comparison of (a,b) hydrogen charged, against (c,d) charged and aged samples as a function of the heating rate. Note that the vertical scale for (c,d) is magnified relative to (a,b).
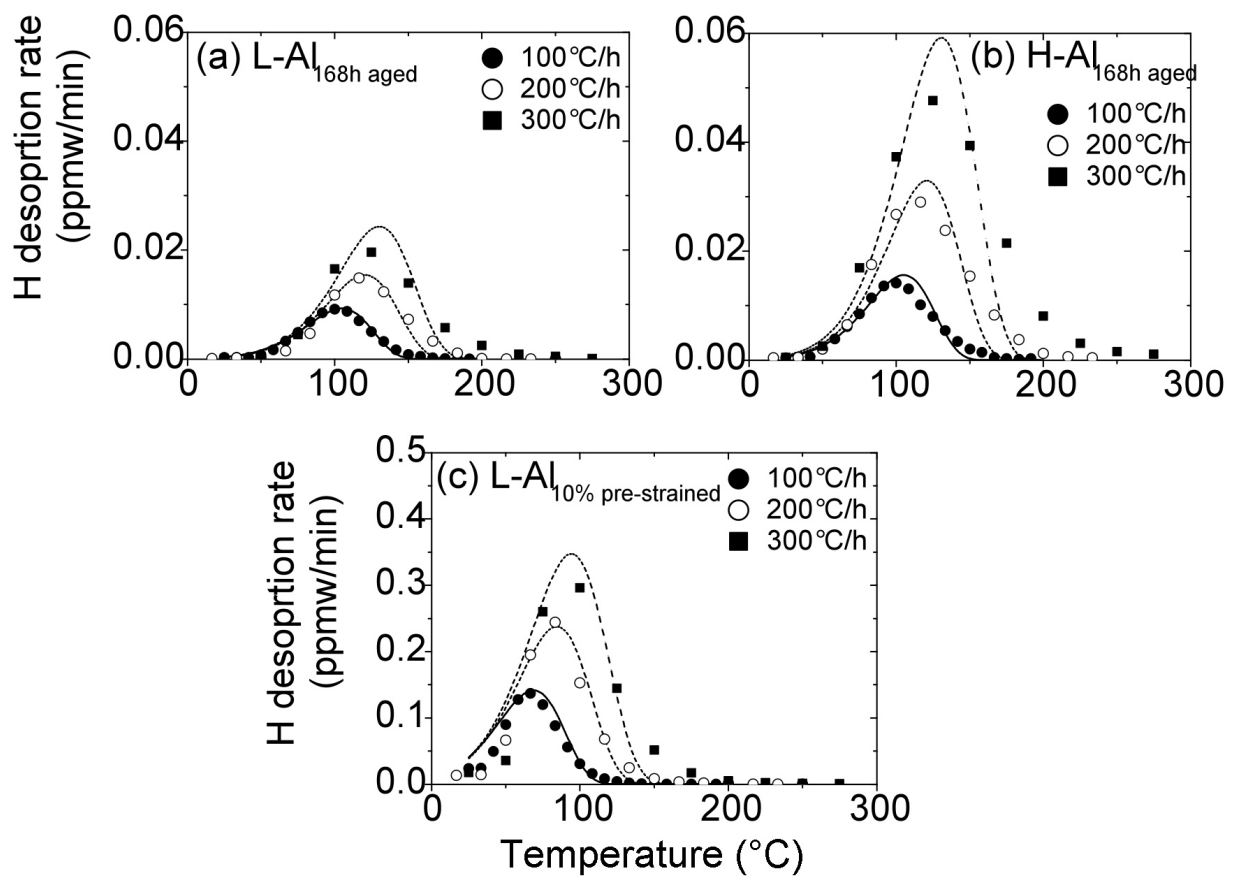
Figure 6: (a,b) Charged and aged samples. Experimental data (points) for $100\,°C\,h^{-1}$ fitted (continuous curves) using a stepwise application of equation 1 together with predicted dashed–curves for the other two heating rates. (c) Similar data and fit for a sample strained 10% prior to TDS measurements.
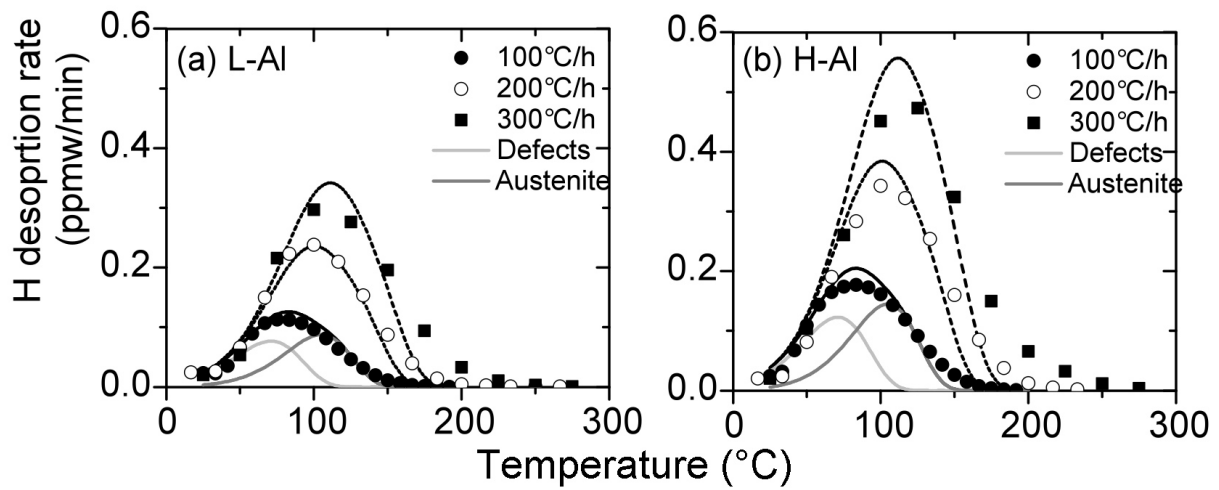
Figure 7: Saturation charged specimens in which the $100\,^\circ\mathrm{C}\,\mathrm{h}^{-1}$ data are used to determine the partitioning of hydrogen trapped in austenite and defects, and the remaining heating rate curves (dashed) are predicted.
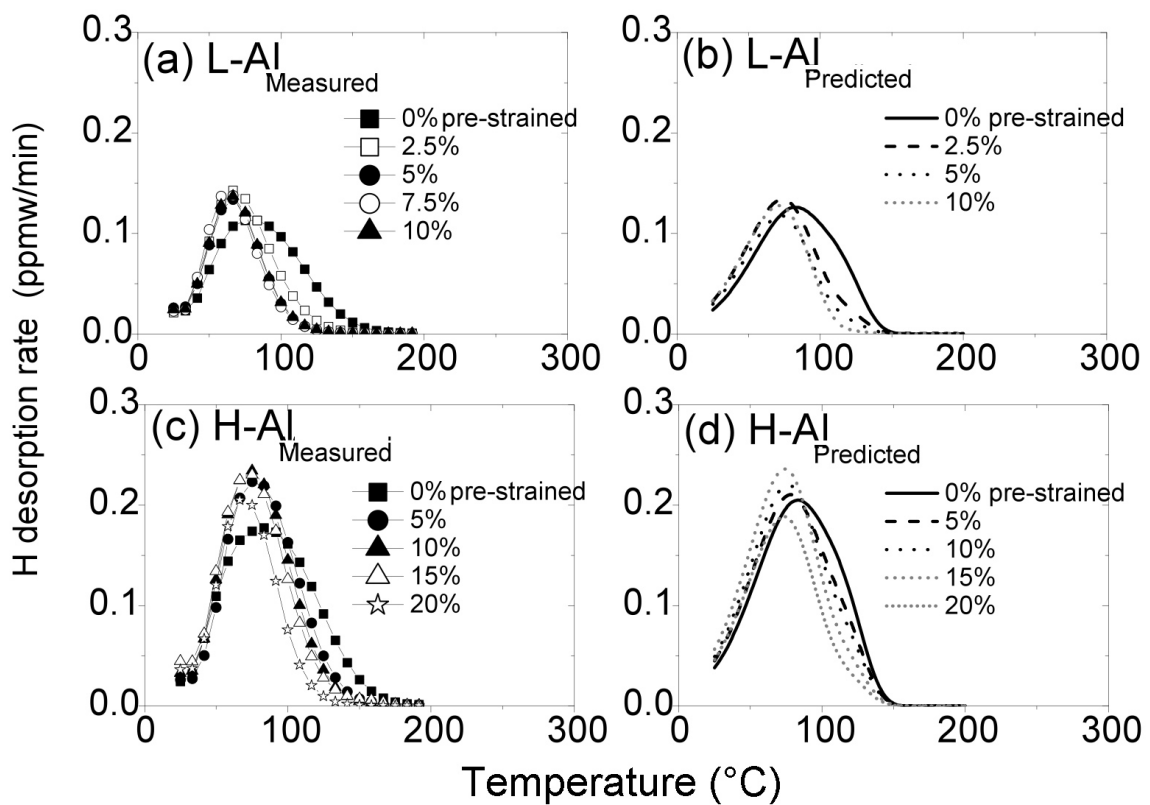
Figure 8: Measured (a,c) and predicted (b,d) thermal desorption spectra for samples strained prior to saturation hydrogen–charging.
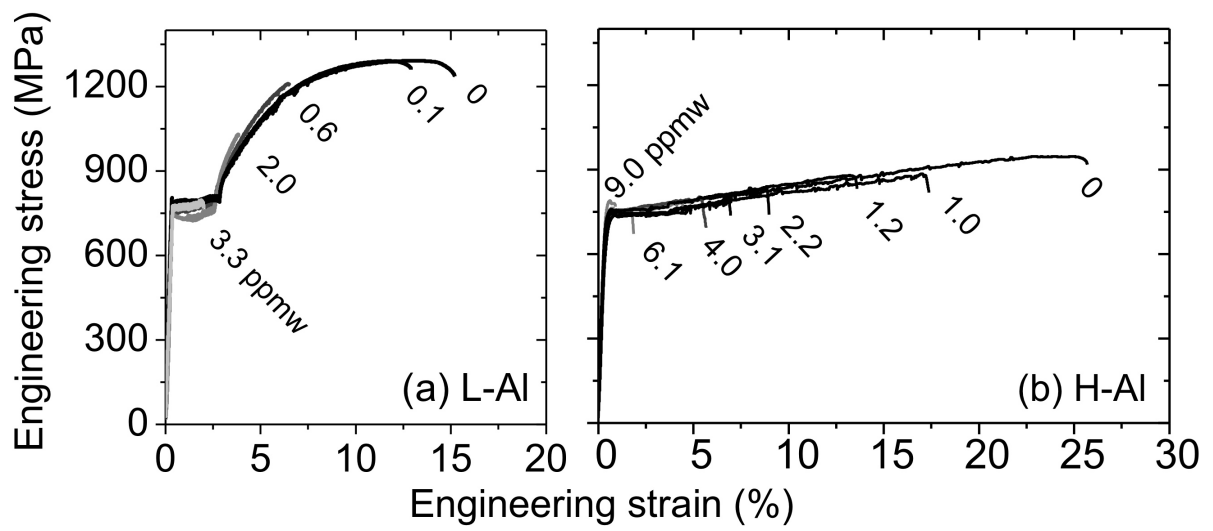
Figure 9: Stress–strain curves of pre–charged (a) L–Al and (b) H–Al alloys tested at a strain rate of $10^{-5}\,\mathrm{s}^{-1}$. Diffusible hydrogen contents in specimen are labelled in ppmw.
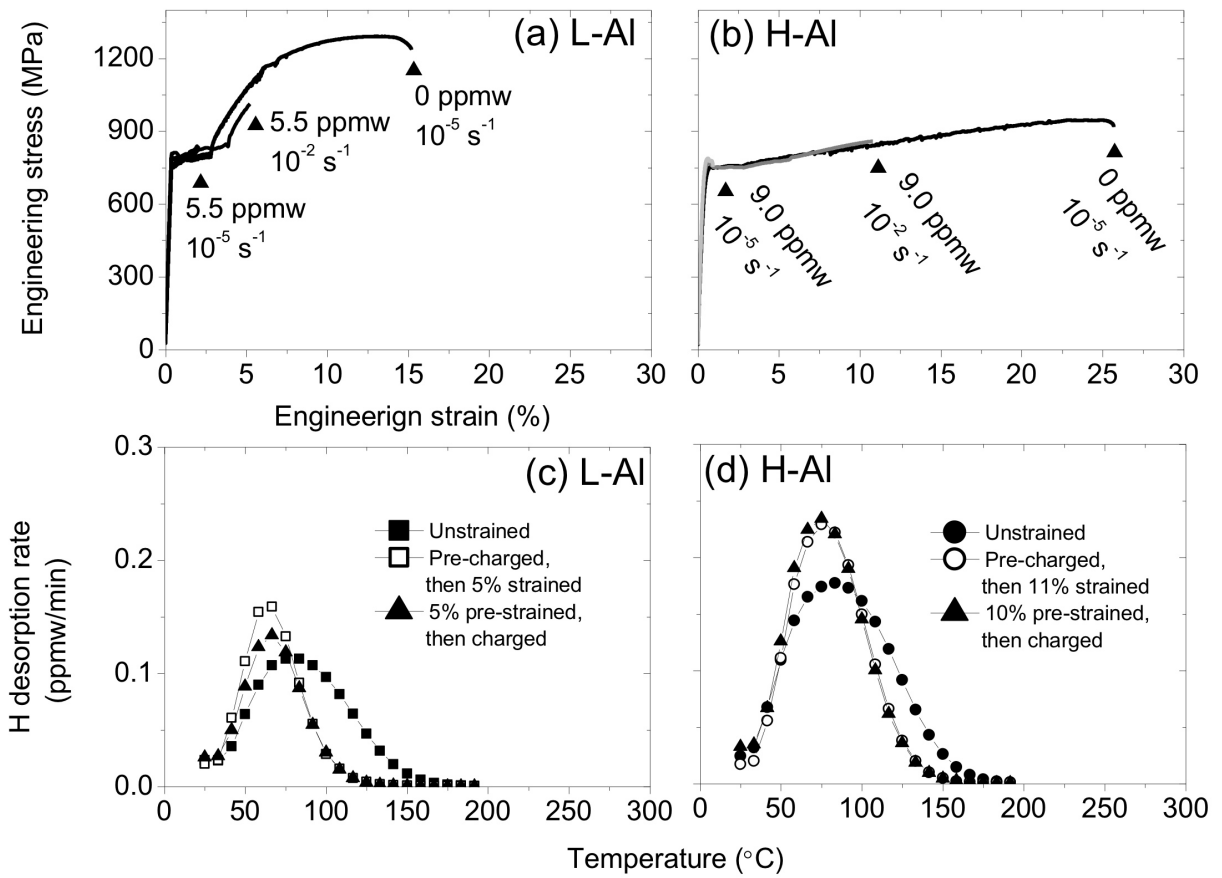
Figure 10: Stress-strain curves of (a) L-Al and (b) H-Al alloys tested at different strain rates. Thermal desorption profiles of (c) L-Al and (d) H-Al alloys. Pre-charged and then strained specimens are compared with pre–strained and then charged ones.

[1] Oriani, RA, Josephic, PH. Acta Metallurgica 1974;22:1065–1074.

[2] Hirth, JP. Metallurgical & Materials Transactions A 1980;11(861–890).

[3] Kushida, T, Kuratomi, N, Kudoh, T, Matsumoto, H, Tsumura, T, Nakasato, F. Tetsu–to–Hagane 1996;82:297–302.

[4] So, KH, Kim, JS, Chun, YS, Park, KT, Lee, YK, Lee, CS. ISIJ International 2009;49:1952–1959.

[5] Loidl, M, Kolk, O, Veith, S, Göbel, T. Materialwissenschaft und Werkstofftechnik 2011;42:1105–1100.

[6] Kim, JS, Lee, YH, Lee, DL, Park, KT, Lee, CS. ISIJ International 2007;47:913–919.

[7] Bhadeshia, HKDH. Progress in Materials Science 2012;57:268–435.

[8] Tsubakino, H, Harada, H, Yin, J. ISIJ International 1999;39:298–300.

[9] Hojo, T, Sugimoto, K, Mukai, Y, Ikeda, S. ISIJ International 2009;48:824–829.

[10] Escoba, DP, Duprez, L, Verbeken, K, Verhaege, M. in: Somerday, PSB, Jones, R, (eds.) Effects of Hydrogen on Materials. Ohio, U. S. A.: ASM International; 2009, 485–492.

[11] Suh, DW, Park, SJ, Lee, TH, Oh, CS, Kim, SJ. Metallurgical & Materials Transactions A 2010;41:397–408.

[12] Jatczak, CF. SAE Technical Paper Series 1980;800426:1–19.

[13] Subcommittee, , E28-04, . Standard test methods for tension testing of metallic materials. ASTM E8M–03; 2003.

[14] Ryu, JH, Kim, DI, Kim, HS, Bhadeshia, HKDH, Suh, DW. Scripta Materialia 2010;63:297–299.

[15] Pressouyre, GM, Bernstein, IM. Metallurgical transactions A 1978;9:1571–1580.

[16] Takai, K, Watanuki, R. ISIJ International 2003;43:520–526.

[17] Murakami, Y, Kanezaki, T, Mine, Y, Matsuoka, S. Metallurgical & Materials Transactions A 2008;39:1327–1339.

[18] Kiuchi, K, McLellan, RB. Acta Metallurgica 1983;31:961–984.

[19] Martinez-Madrid, M, Chan, SLI, Charles, JA. Materials Science and Technology 1985;1:454–460.

[20] Kissinger, HE. Analytical Chemistry 1957;29:1702–1706.

[21] Yamaguchi, T, Nagumo, M. ISIJ International 2003;43:514–519.

[22] Xiukui, S, Jian, X, Yiyi, L. Materials Science & Engineering A 1989;114:179–187.

[23] Choo, WY, Lee, JY. Metallurgical Transactions A 1982;13:135–140.

[24] Mine, Y, Horita, Z, Murakami, Y. Acta Materialia 2009;57:2993–3002.

[25] Ulmer, DG, Altstetter, CJ. Acta Metallurgica and Materialia 1993;41:2235–2241.

[26] Rozenak, P, Bergman, R. Materials Science & Engineering A 2006;437:366–378.

[27] Asano, S, Otsuka, R. Scripta Metallurgica 1976;10:1015–1020.

[28] Bernstein, IM. Materials Science and Engineering 1970;6:1–19.